Electrochemical impedance spectroscopy of a reverse electrodialysis stack

Journal of Power Sources 444 (2019) 227302

Contents lists available at ScienceDirect

Journal of Power Sources

journal homepage: www.elsevier.com/locate/jpowsour

Electrochemical impedance spectroscopy of a reverse electrodialysis stack: A new approach to monitoring fouling and cleaning

Diego Pintossi [a,b], Michel Saakes [a], Zandrie Borneman [b,c], Kitty Nijmeijer [b,c,*]

[a] Wetsus, European Centre of Excellence for Sustainable Water Technology, P.O. Box 1113 8900 CC, Leeuwarden, the Netherlands
[b] Membrane Materials and Processes, Department of Chemical Engineering and Chemistry, Eindhoven University of Technology, P.O. Box 513, 5600 MB Eindhoven, the Netherlands
[c] Dutch Institute for Fundamental Energy Research (DIFFER), PO Box 6336, 5600 HH Eindhoven, the Netherlands

HIGHLIGHTS

- Novel real-time fouling monitoring method for reverse electrodialysis.
- Suitable for monitoring results of stack cleaning procedures after fouling.
- Enabling efficient cleaning for reverse electrodialysis with natural feedwaters.

GRAPHICAL ABSTRACT

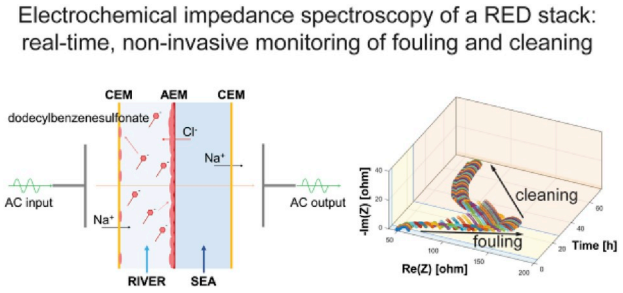

ARTICLE INFO

Keywords:
Reverse electrodialysis
Fouling
SDBS
EIS
Salinity gradient energy

ABSTRACT

When harvesting salinity gradient energy via reverse electrodialysis (RED), stack performance is monitored using DC characterizations, which does not provide information about the nature and mechanisms underlying fouling inside the stack. In order to assess the potential of natural salinity gradients as renewable energy source, progress in the fields of fouling monitoring and controlling is vital. To improve fouling and cleaning monitoring, experiments with sodium dodecylbenzenesulfonate (SDBS) were carried out while at the same time the electrochemical impedance spectroscopy (EIS) was measured at the RED stack level. EIS showed how SDBS affected the ohmic resistance of the stack, the non-ohmic resistance of the AEM and the non-ohmic resistance of the CEM on different time scales. Such detailed investigation into the effect of SDBS on different stack elements offered by EIS is not possible with traditional DC characterization. The results presented in this work illustrate the potential of EIS at the stack level for fouling monitoring. The knowledge presented shows the possibility to include EIS in upscaled natural salinity gradient RED applications for fouling monitoring purposes.

1. Introduction

To harvest salinity gradient energy, reverse electrodialysis (RED) is a promising technology that generates electricity by controlled mixing of aqueous solutions with different salinities, such as river water and seawater [1]. RED uses non-porous ion exchange membranes (IEMs) that are permselective for cations (cation exchange membranes, CEMs) or anions (anion exchange membranes, AEMs). The IEMs are stacked alternately with high salt concentration and low salt concentration

* Corresponding author. Membrane Materials and Processes, Eindhoven University of Technology, P.O. Box 513, 5600 MB Eindhoven, the Netherlands.
E-mail address: d.c.nijmeijer@tue.nl (K. Nijmeijer).

https://doi.org/10.1016/j.jpowsour.2019.227302
Received 15 July 2019; Received in revised form 10 October 2019; Accepted 12 October 2019
Available online 22 October 2019

Glossary

AC	Alternating current
AEM	Anion exchange membrane
CEM	Cation exchange membrane
CPE	Constant phase element
DC	Direct current
EEC	Electrical equivalent circuit
EIS	Electrochemical impedance spectroscopy
I	Current
IEM	Ion exchange membrane
j	Imaginary unit
R	Resistance
RED	Reverse electrodialysis
RW	River water
SDBS	Sodium dodecylbenzenesulfonate
SDS	Sodium dodecylsulfonate
SW	Seawater
t	Time
U	Potential
Z	Impedance
ϕ	Phase shift
ω	Angular frequency

feedwaters flowing on either side along the membranes [2]. The difference in salt concentration between the feedwaters creates a potential difference across the membranes [3]. At the two ends of the stack, electronic redox reactions convert the ionic current into an electric current. The generated electrical current can then be used to power an external load [4].

In order to be able to use RED as a renewable energy source for a long time, fouling is one of the main challenges to be addressed [5]. There are many different forms of fouling affecting RED: colloidal fouling, inorganic fouling (scaling, uphill transport of multivalent cations like Ca^{2+} and Mg^{2+} and poisoning of the membranes due to multivalent ions), organic fouling and biofouling [6–8]. Although there are similarities with membrane fouling in water treatment, the nature, interactions and consequences are distinctively different in RED due to the use of charged anionic and cationic membranes, and the transport of ions instead of water molecules as in water treatment and purification [9].

In the natural environment and in laboratories, the study of fouling phenomena in RED happened at two levels: the stack level and the single membrane level. This approach on two different levels reflects the trade-off existing in RED fouling investigations: either a highly representative system where the available characterization tools are limited by the system intrinsic complexity (stack level) or a simplified system that allows more flexibility in terms of available characterizations techniques but at the same time does not truly reflect the hydrodynamic and physical conditions found in real, natural water, RED systems (membrane level). For the RED stack, electrolyte compartments, water compartments and membranes all contribute to the system performance. The traditional DC characterization applied at stack level implies a black box approach, where the overall behavior of the system is measured without the possibility to investigate in a non-destructive way the impact of fouling on the CEM or AEM in detail. Therefore, studies at the stack level monitor the effect of fouling on the complete stack, rather than monitoring fouling evolution and dynamics, relying on the evolution over time of electrochemical parameters, like open circuit voltage and stack electrical resistance, and other parameters, like pressure drop between feedwaters inlets and outlets [6,10]. Even a new stack design based on the idea of dividing the RED stack in two halves allowing the monitoring of single membranes without affecting the hydrodynamics in the water compartment relies on the same DC characterization, thus limiting the amount of information that is extracted in real time from individual membranes in the stack [11]. Studies at the membrane level offer a wider set of available characterization techniques, including electrochemical impedance spectroscopy (EIS). The advantage of EIS over DC characterization is the possibility to investigate individual components that all contribute to the overall resistance. At membrane level, EIS was used to distinguish the contributions to the membrane resistance of membrane bulk, electrical double layer, diffusion boundary layer and fouling in clean or foulants containing water [12–21]. EIS enables the detailed observation of the effect of fouling not just on the overall resistance, but also how the fouling layers hinders ion transport in the diffusion boundary layer. However, studies at the membrane level are often carried out in systems with wide water compartments, where the absence of spacers and configuration of the inlets and outlets lead to very different flow and current fields over the membrane. Since flow and current fields have a huge influence on the fouling evolution of AEMs, results obtained in these studies at the membrane level cannot be directly translated into knowledge of membrane behavior inside the stack. Performing EIS at the stack level moves fouling monitoring and analysis in RED beyond the present trade-off. EIS at stack level unravels detailed information on how fouling builds up on the anion and cation exchange membranes in a highly representative RED stack environment, enabling real time and non-destructive fouling monitoring. RED stacks have a large capacitance due to large electrode-electrolyte and membrane-electrolytes interfaces. This leads to long EIS measurement times since the characteristic frequencies of systems with large capacitance are very low. Long measurement times in a fouling experiment make it difficult to assume steady-state of the system during the EIS scan. That is because the system performance deteriorates considerably over the scan time due to fouling, leading to the characterization of a system that changes significantly throughout the measurement, thus impairing the significance of the measured data. Additionally, when correctly measured, the meaning of impedance spectra of a stack needs to be unraveled to attribute spectral features to the single stack elements, namely electrodes and electrolyte, membranes and water compartments. Overcoming such issues is not trivial, as highlighted by the scarcity of studies reporting EIS at the stack level. Modulation of the active membrane area to limit interfacial capacitance is a promising strategy to reduce EIS measurement time and enable EIS at the stack level. In the RED literature, the only example of EIS at the stack level is provided by Choi et al., who studied the effect of process parameters like flow rate and salt concentration on the RED performance in a small area stack with one cell pair [22]. Thanks to EIS, they could study the dependence of the resistance components on the process parameters under study.

This paper presents the use of EIS at the stack level for fouling monitoring and characterization. The modulation of active membrane area is the key to enable the measurement of impedance spectra at the stack level. To interpret spectra, a step-by-step procedure was adopted analyzing systems with increasing complexity, moving from a relatively simple system consisting of the electrodes and electrolyte to the full RED stack. A model compound, sodium dodecylbenzenesulfonate (SDBS) was used for fouling experiments. EIS successfully tracks fouling and cleaning in the stack, with more information on the interaction between the model compound and the membranes than the traditional DC characterization. Finally, based on the information provided by EIS, a mechanism for the evolution of fouling on the membranes is proposed. These results prove the feasibility of EIS as a tool for real-time and non-destructive fouling monitoring at the stack level, revealing how the foulants absorb in and adsorb on the ion exchange membranes, thus paving the way for tailored cleaning strategies, where the consumption

of cleaning resources is minimized while maximizing their effect.

2. Theory

The underlying principle of electrochemical impedance spectroscopy is the application of a sinusoidal input to an electrochemical system, like a RED stack, and measurement of the corresponding sinusoidal output or response of the system under study. Such a process is repeated for a large set of frequencies, to identify phenomena that occur at different characteristic frequencies. As input, a current is employed with potential measured as the output, or vice versa. Input and output are sinusoidal functions with the same frequency, but their amplitudes differ. Additionally, whenever the system under investigation has a capacitive or inductive behavior, the output signal is characterized by a phase shift ϕ with respect to the input signal (Figure S1). Considering Ohm's law for a DC characterization:

$$U = R\,I \tag{1}$$

where U is the potential [V], R is the electrical resistance [Ω] and I is the current [A], a similar approach is adopted for EIS. Having a sinusoidal voltage as an input:

$$U(\omega,t) = U_0 sin(\omega t) = U_0 e^{j\omega t} \tag{2}$$

with U_0 the amplitude of the oscillation [V], j the imaginary base vector, ω the angular frequency ($\omega = 2\pi f$, where f is the frequency [Hz]) and t the time [s], the measured output will be:

$$I(\omega,t) = I_0 sin(\omega t + \phi) = I_0 e^{j(\omega t+\phi)} \tag{3}$$

where I_0 is the amplitude of the measured sinusoidal current. The relationship between the two quantities is given by a quantity called impedance:

$$Z(\omega) = \frac{U(\omega,\ t)}{I(\omega,\ t)} = \frac{U_0 e^{j\omega t}}{I_0 e^{j(\omega t+\phi)}} = |Z| e^{-j\phi} \tag{4}$$

It can be noted that the time dependency is lost when calculating the ratio between alternating voltage and alternating current. Thus, impedance is a time-independent quantity. However, impedance depends on frequency since the phase shift ϕ depends on frequency. For a time-independent impedance measurement, the electrochemical system under investigation should be linear and steady-state, at least for the duration of the EIS measurement. For IEMs, modeling and experimental work has been carried out to measure the impedance spectrum of single membranes [23,24]. The typical electrical equivalent circuit (EEC) for a single IEM is represented in Figure S2. The contribution from bulk of the membrane, electrical double layer and diffusion boundary layer to the membrane resistance can be identified based on their different characteristic frequencies. Since membrane resistance implies the conduction of ions, ionic movement at a longer scale results in a lower characteristic frequency for the spectral feature associated to that motion. The first element in the equivalent circuit, a resistor, represents the ohmic component of the membrane impedance (purely resistive behavior measured at high frequencies), the second element, a parallel of a resistor and capacitor, stands for the impedance of the electrical double layer (measured at intermediate frequencies, since it involves the migration of ions at the nanometer scale), while the last element, a parallel connection of a resistor and a CPE, represents the impedance of the diffusion boundary layer (measured at low frequencies, since it involves the diffusion of ions at the micrometer scale) [14,17].

For complex electrochemical systems, such as a RED stack, multiple phenomena contribute to a single spectral feature. Therefore, a single arc may result from the convolution of multiple arcs deriving from different phenomena.

3. Materials and methods

3.1. Materials

For the experiments, demineralized water (produced by an Osmostar S400, Lubron Waterbehandeling BV, the Netherlands) was used. Sodium chloride (NaCl, 99.5% purity, ESCO, the Netherlands) and sodium dodecyl benzene sulfonate (SDBS, technical grade, Sigma-Aldrich, Germany) were used as solutes. Potassium hexacyanoferrate(II) trihydrate and potassium hexacyanoferrate(III) (both technical grade, at least 96% purity, VWR Chemicals, Belgium) were used as electrolytes.

For the stack assembly, the chosen AEMs and CEMs were homogeneous standard grade Fujifilm AEM type I (FUJIFILM Manufacturing Europe BV, the Netherlands) and homogeneous standard grade Neosepta CMX-fg (ASTOM Corp. Ltd., Japan), respectively. Neosepta AMX-fg was used as alternative AEM to investigate the effect of different AEMs on the impedance spectrum.

3.2. Stack configurations

The experiments were performed with cross-flow RED stacks (REDstack BV, the Netherlands) with an active area of $10 \times 10\ cm^2$. The stack end plates embedded platinized titanium mesh electrodes ($9.8 \times 9.8\ cm^2$) (MAGNETO Special Anodes BV, the Netherlands). Spacers with a woven netting (Sefar 06-700/53, Sefar AG, Switzerland) and integrated silicone rubber gaskets with a custom design (AquaSEAL by AquaBattery, the Netherlands) were used to accommodate the feedwaters, seal the compartments, and reduce the active area of the cell from 100 cm^2 to 4 cm^2 and 1 cm^2. Two active areas and four different configurations were used to enable the interpretation of the impedance spectra of the RED stack. This approach made it possible to compare impedance spectra of similar systems of increasing complexity. These stack configurations are summarized in Table 1.

The configurations with one CEM are represented in Figure S3, while Figure S4 depicts the complete RED stack configuration with a complete cell pair consisting of a CEM, a river water compartment, an AEM, a seawater compartment, another sealing CEM, and the electrolyte compartments at both ends of the stack.

3.3. Feedwaters and electrolyte

NaCl solutions of 0.017 M and 0.508 M were used as artificial river water and seawater, respectively. 50 ppm and 100 ppm SDBS was added

Table 1
Summary of the stack configurations used in the present work. Electrolyte solution is recirculated in the electrode compartments for all configurations. RW stands for river water compartment, SW stands for seawater compartment, N stands for no addition and Y stands for yes addition of SBDS.

Name	Area	CEM	AEM	RW	SW	SDBS	Aim
a	1 cm^2	0	0	0	0	N	Determine impedance of electrodes with reduced open area.
b	1 cm^2	1	0	0	0	N	Determine the impedance of electrodes separated by one CEM, with reduced active membrane area.
c	4 cm^2	1	0	0	0	N	Determine the effect of active membrane area on the impedance of system made of electrodes separated by one CEM.
d	1 cm^2	2	1	1	1	N	Study of complete RED stack impedance.
e	1 cm^2	2	1	1	1	Y	Monitoring of fouling and cleaning.

to the river water for the fouling experiments. SDBS was chosen as a model compound for organic fouling of the AEM, as it is known to interact with the membrane on a relatively short time scale, severely affecting the membrane properties [25,26]. Solutions of 0.05 M potassium hexacyanoferrate(II)/0.05 M potassium hexacyanoferrate(III) were used as electrolyte. Sodium chloride (0.25 M) was added as a supporting electrolyte. Experiments were performed in the laboratory at 23.0 ± 0.5 °C. Temperature and conductivity of the artificial feedwaters were monitored before each experiment. The flow velocity was chosen to be 1 cm/s. Fresh feedwaters were continuously supplied to the RED stacks, in a single-pass configuration, while the electrolyte was recirculated in a closed loop. Peristaltic pumps (Masterflex L/S Digital drive, Cole-Palmer, USA) were used to pump the liquids through the hydraulic circuits. The electrolyte was kept at 0.3 bar overpressure using a diaphragm pressure control valve (KNF FDV 30, KNF-Verder BV, the Netherlands) to avoid bulging of the water compartments.

Configurations a-d in Table 1 were used to study the impedance spectra of the clean RED stack and understand their meaning by breaking down the systems in simpler configurations. In addition to those experiments, two more sets of experiments were carried out with configuration e in Table 1: 1) a fouling experiment, and 2) a fouling and cleaning experiment. For the fouling experiment, clean feedwaters containing only sodium chloride were supplied to the stack in the initial phase of the fouling experiment. Subsequently, clean river water was substituted with river water containing 50 ppm SDBS. Finally, the SDBS concentration in the river water was increased to 100 ppm. For the fouling and cleaning experiment, clean feedwaters containing only sodium chloride were supplied to the stack in the first step of the experiment. Then, clean river water was substituted with river water containing 100 ppm SDBS. Finally, clean river water containing only sodium chloride was supplied to the stack after fouling as a cleaning method.

3.4. Electrochemical measurements and data analysis

All electrochemical measurements were performed with an Autolab PGSTAT302 N (Metrohm Autolab BV, the Netherlands). The software NOVA 2.1.3 was used to control the potentiostat. Electrochemical measurements were continuously repeated in a loop. A loop cycle consisted of one constant current step (10 A/m^2, galvanostatic mode), a chronopotentiometric series consisting of three current steps separated by open circuit steps (5, 10 and 15 A/m^2, galvanostatic mode), a second constant current step, a second chronopotentiometric series and, finally, an EIS scan (100 kHz–10 mHz, 10 mV amplitude superimposed to a constant voltage equal to half of the open circuit voltage, potentiostatic mode). The choice of the frequency range was based on literature values and process conditions [16–19]. It is important to have a relatively fast impedance scan, otherwise the system will change considerably due to fouling or cleaning during the scan time. The galvanostatic mode, where the current is the input to the system and the voltage is the measured output, was chosen for the DC measurements since it is well established in RED literature [27–29]. The potentiostatic mode, where voltage is the input and current is the output from the system, was chosen for the AC measurement. A graphical representation of the current evolution during one measurement loop is provided in Figure S5. The duration of one loop cycle was approximately 1 h. The open circuit voltage (OCV) was evaluated in the open circuit steps at the beginning of each chronopotentiometric series. Stack electrical resistance was evaluated from the slope of the I–V curve obtained from the chronopotentiometric series. The design of the experiment allowed the comparison of stack electrochemical indicators measured in DC mode (chronopotentiometric series) and AC mode (EIS). Matlab software (The MathWorks Inc., USA) was used for data analysis. Scripts were developed for the specific purpose of processing the data from the chronopotentiometric series and EIS scans. For the analysis of EIS data, the Zfit script [30], which performs fitting of experimental impedance data with a determined equivalent circuit, was integrated into our analysis procedure.

4. Results and discussion

In the next parts impedance spectra for a pristine, fouled and a cleaned RED stack are discussed to prove the feasibility of EIS at the stack level for fouling monitoring purposes.

4.1. EIS spectrum of the pristine RED stack

To enable EIS at the stack level, the key is reducing the overall capacitance of the system as this otherwise highly dominates characteristic frequencies and measurement time. Since the capacitance of the system is mostly due to electrical double layers at the membrane-solution interfaces, reducing the active membrane area decreases the overall system capacitance. This leads to higher characteristic frequencies, thus faster measurements. To evaluate this strategy, specially designed gaskets were employed in the electrolyte and water compartments (Figure S4). Two active membrane areas were used: 4 cm^2 and 1 cm^2. Fig. 1 presents the spectra for a simplified system comprising of only electrodes separated by one CEM (Figure S3), measured for the two different active areas.

In accord with the theory we found that the characteristic frequencies for the two arcs are higher for the system with the smaller active area (blue squares) than those of the system with the larger active area (red circles). Therefore, the use of special gaskets to reduce the active area was effective to enable fast EIS measurements at the stack level.

In Fig. 1, for all system configurations, with and without a CEM separating the electrodes, the EIS spectra comprise two arcs. The smaller arc at high frequencies is almost constant for the two active areas, while the arc at lower frequencies changes considerably with the active area. The width on the real component axis (*x*-axis) of the lower frequency arc and its height on the imaginary component axis (*y*-axis) are larger for the smaller active membrane area. Such behavior suggests that the high frequency arc is related to the electrodes, while the lower frequency arc is related to the CEM. To investigate if the electrodes also affect the

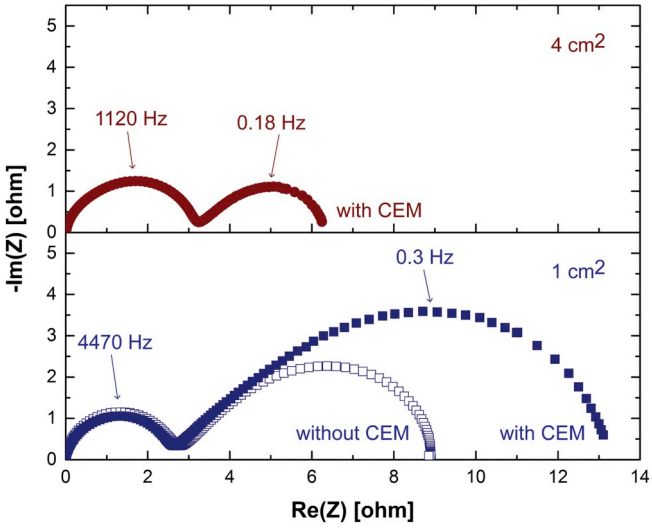

Fig. 1. Nyquist plots for the electrode system with or without a CEM in between: red circles represent the system with 4 cm^2 active area comprising a CEM between the electrodes, empty blue squares represent the system with 1 cm^2 active area without a CEM between the electrodes, filled blue squares represent the system with 1 cm^2 active area comprising a CEM between the electrodes. The ohmic component of the spectra (intercept with x-axis at high frequencies) was subtracted for ease of comparison. (For interpretation of the references to colour in this figure legend, the reader is referred to the Web version of this article.)

lower frequencies arc, an additional measurement was performed with the 1 cm^2 system but without the CEM. The resulting spectrum shows two arcs representing the impedance of the charge transfer step at the electrode-electrolyte interface (high frequency response) and the mass transfer from the open area to the masked portion of the electrodes (lower frequency response). Comparing the spectra of the systems with and without the CEM, the effect of the membrane on the EIS spectrum is evident. Therefore, the high frequency arc is mainly dictated by the electrodes, while the low frequency arc combines both the electrodes and the CEM.

Fig. 2 shows the measured spectrum for the one cell-pair RED stack (a CEM, a AEM/CEM pair and the electrodes) with 1 cm^2 active membrane area.

When comparing the spectrum of the complete RED stack (Fig. 2) with that of the electrodes separated by one CEM only (Fig. 1), a small third arc at high frequencies is visible (Fig. 2, inset). This newly created high frequency arc is caused by the additional AEM. Also, the size of the corresponding arcs has changed and the electrode arc in Fig. 1 has increased in Fig. 2. This indicates that the addition of an AEM also influences that the low frequency arc. Therefore, in the complete RED stack this second arc is the convolution of the AEM and electrode response. To further verify this conclusion, another stack comprising a different AEM was assembled. Figure S6 shows the spectra for the two complete RED stacks one with a Fujifilm AEM type I and one with a Neosepta AMX-fg membrane. Also in Figure S6 shows that changing the AEM affects the ohmic resistance and both arcs at high frequencies, thus confirming the influence of the AEM on both arcs. For the low frequency arc, the difference is that in Fig. 1 only one CEM and in Fig. 2 two CEMs are used. Since the two CEMs are assumed to have similar impedances, their spectra will coincide resulting in one larger arc derived from the convolution of the two single CEM arcs. This is the case for the low frequency arc in Fig. 2.

With these results we now show the impedance spectrum of a full RED stack. Moreover, systematic build-up of the RED stack and measurement of the corresponding spectra allows the detailed identification of the contribution of each single stack element.

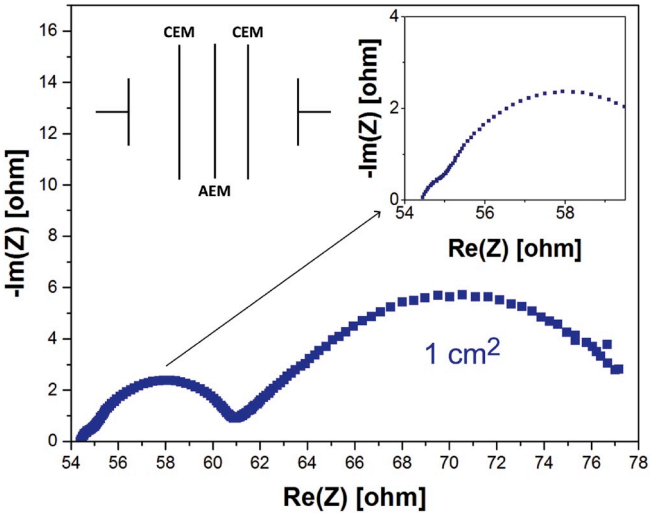

Fig. 2. Nyquist plot for the one cell-pair RED stack (a CEM, an AEM/CEM pair and the electrodes) with 1 cm^2 active membrane area. The inset highlights the high frequency region displaying the small arc attributed to the AEM. For this plot for the complete stack, the ohmic component of the resistance (high frequency intercept with the x-axis) is not subtracted, since this spectrum represents the starting point for the fouling experiments, making the ohmic component a relevant parameter. (For interpretation of the references to colour in this figure legend, the reader is referred to the Web version of this article.)

4.2. Fouling experiment

Subsequently, we used EIS to characterize fouling at the stack level using SDBS as model foulant.

Fig. 3 shows the electrical resistance of the RED stack measured in DC.

The adsorption of SDBS on the membranes and in the stack resulted in an increase in electrical resistance. At 50 ppm SDBS in river water, fouling is limited and the stack electrical resistance plateaus at 84.7 Ω (+7.4%). At 100 ppm SDBS, fouling is more severe, with the stack electrical resistance reaching 195.4 Ω (+147%). Although interesting, DC characterization at the stack level does not provide information about the specific location of the fouling in the stack. Since SDBS is a negatively charged model compound, the main contribution to the increased electrical resistance was due to fouling of the AEM. Where DC is unable to discriminate between the different components in the stack, EIS does have that possibility expanding the investigation of fouling in RED towards a previously impossible extension.

Fig. 4 shows the corresponding EIS data in time (Figure S8 and Figure S9 present the corresponding Bode and Nyquist plots).

Upon fouling, the ohmic component of the stack (ohmic resistance of the AEM, the CEM, the water compartments and the electrodes) impedance increases (from initially 54.5 Ω to more than 100 Ω after 60 h of fouling). Fig. 5 shows the evolution of this ohmic resistance over time. This increase is caused by the SDBS absorbing in the AEM, where it binds to the quaternary ammonium groups. The lower ion exchange capacity (IEC) and free volume available for ion transport determine such increase in electrical resistance.

For the pristine stack, the model (Equation S(11)) predicts an ohmic resistance of 53.0 Ω, compared to the experimental value of 54.5 Ω measured experimentally. The contribution of the AEM is only 1.1 Ω. At the end of the fouling experiment, the ohmic resistance is 115.4 Ω (+112%). This increase mostly stems from an increase in AEM ohmic resistance [25,26]. The 60-fold increase in membrane resistance is close to results from the literature, where 40-fold and 50-fold increases are reported, due to absorption and surface adsorption of SDBS forming micelles [19,31].

Fig. 6 shows the fitting values for the RQ element describing the AEM non-ohmic resistance in EEC_2 (Figure S7) and its capacitance over time.

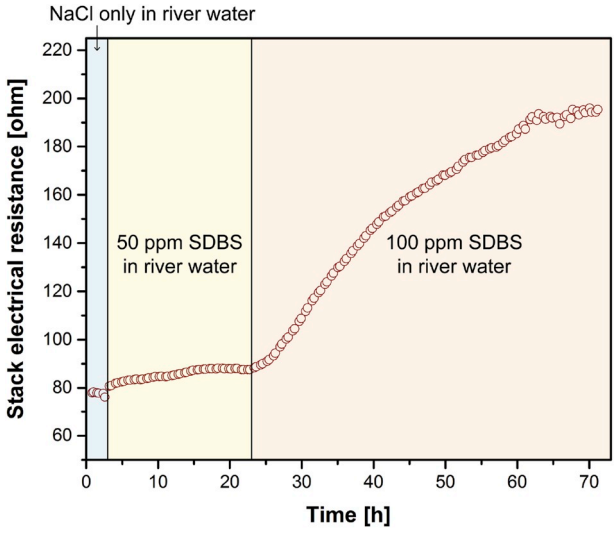

Fig. 3. Evolution of the RED stack resistance over time during the fouling experiment. Blue background: clean river water (0.017 M NaCl). Yellow background: 0.017 M NaCl + 50 ppm SDBS in river water. Orange background: 0.017 M NaCl + 100 ppm SDBS in river water. (For interpretation of the references to colour in this figure legend, the reader is referred to the Web version of this article.)

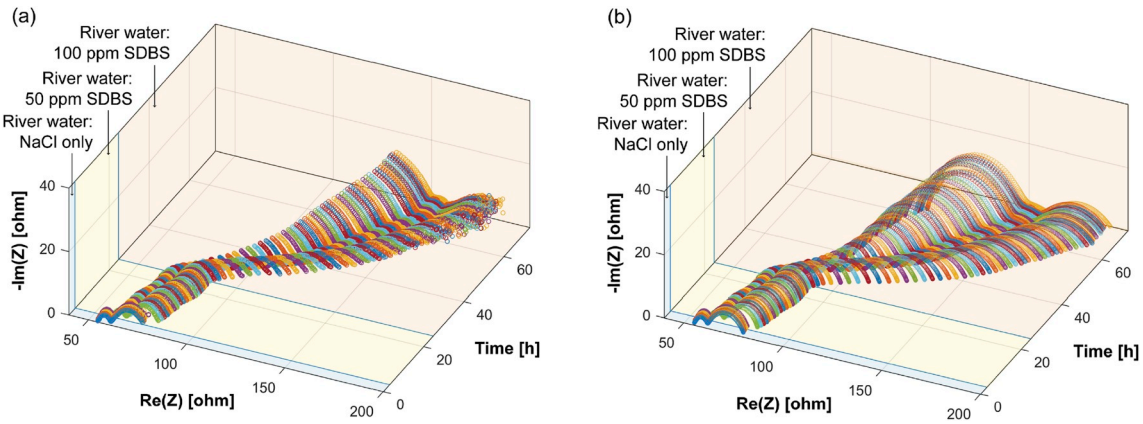

Fig. 4. Evolution of the (a) experimental and (b) EEC_2 model impedance data (Nyquist plot) over time during the fouling experiment. Blue background: clean river water (0.017 M NaCl). Yellow background: 0.017 M NaCl + 50 ppm SDBS in river water. Orange background: 0.017 M NaCl + 100 ppm SDBS in river water. For the model, values for frequencies below 10^{-2} Hz and above 10^{5} Hz have been extrapolated. (For interpretation of the references to colour in this figure legend, the reader is referred to the Web version of this article.)

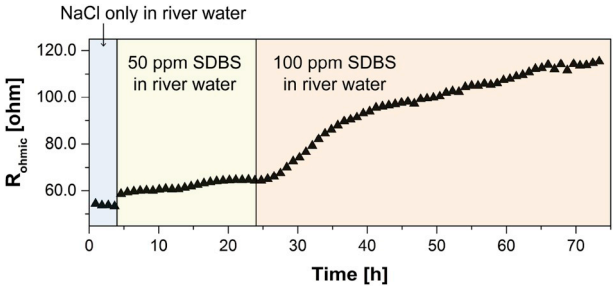

Fig. 5. Evolution of the ohmic resistance (values from EEC fitting of experimental data) over time during the fouling experiment. Blue background: clean river water (0.017 M NaCl). Yellow background: 0.017 M NaCl + 50 ppm SDBS in river water. Orange background: 0.017 M NaCl + 100 ppm SDBS in river water. (For interpretation of the references to colour in this figure legend, the reader is referred to the Web version of this article.)

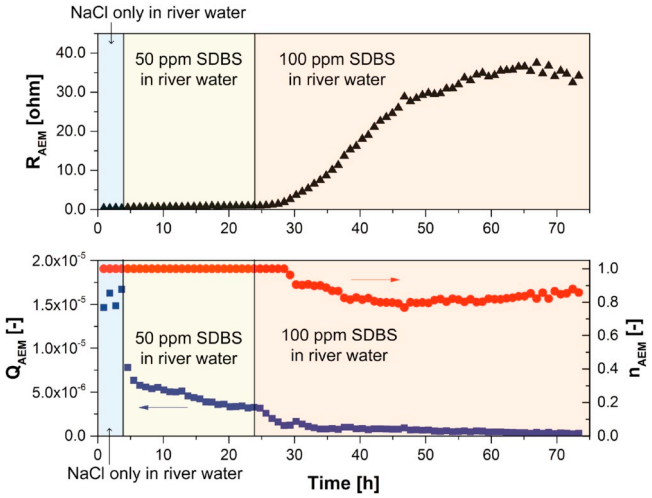

Fig. 6. (Top) Evolution of the non-ohmic AEM resistance (values from EEC fitting of experimental data) over time during the fouling experiment. (bottom) Evolution of the non-ideal capacitance and exponent over time during the fouling experiment for the CPE associated to the AEM. Blue background: clean river water (0.017 M NaCl). Yellow background: 0.017 M NaCl + 50 ppm SDBS in river water. Orange background: 0.017 M NaCl + 100 ppm SDBS in river water. (For interpretation of the references to colour in this figure legend, the reader is referred to the Web version of this article.)

At low concentration of SDBS (50 ppm), the non-ohmic resistance does not significantly increase, while the capacitance associated to the AEM is reduced immediately when SDBS is added to the river water. The capacitance decreases until a plateau value was reached. Increasing the SDBS concentration in the river to 100 ppm water decreased the capacitance further. As soon as the capacitance reaches a plateau, the non-ohmic resistance started to increase until it reached a plateau value at the end of the experiment, reflecting the same trend observed for the overall resistance measured in DC mode. The evolution of non-ohmic resistance and capacitance suggests the formation of SDBS domains on the AEM surface, which negatively affect the double layer capacitance. Over time, these domains grow, thus leading to a further reduction of the AEM capacitance, until a homogenous fouling layer covering the full surface is formed that starts to affect the non-ohmic resistance, slowing down the transport of ions to the membrane. This finding is consistent with previous studies on The formation of SDBS micelle layers and its impact on membrane resistance [19,31]. The phase shift angle peak corresponding to the AEM (Figure S10) element shifts towards higher frequencies over time. This behavior is consistent with a reduction in the active area that is caused by the fouling domains on the AEM surface. This shift is only observed for the AEM, suggesting that SDBS is mostly affecting the AEM.

Fig. 7 shows the evolution of the fitting values for the non-ohmic resistance and capacitance of the mixed electrode-CEM element.

The evolution of the non-ohmic resistance and capacitance of the CEM resembles that of the AEM, although the extent and rate of the non-ohmic resistance increase for the CEM is slower. The capacitance decreased only at high SDBS concentrations, suggesting that SDBS partly also deposited on the CEM, but the domains remain mostly separated since the capacitance did not plateau until the end of the experiment. Fouling of the CEM by the negatively charged SDBS may seem counter-intuitive, but since SDBS was present in the river water compartment, the electric field pushed it towards the anode and thus the CEM. The concentration of SDBS at the CEM surface exceeded locally the critical micelle concentration (CMC) resulting in the local formation of a micellar configuration, shielding the negative charges of SDBS.

4.3. Fouling and cleaning experiment

Finally, the effect of a subsequent cleaning step after a 100 ppm SDBS fouling run is investigated using EIS.

Figure S11 shows the evolution of the stack electrical resistance as measured from the slope of the I–V curve in DC mode. The resistance increase upon fouling was even faster than in the previous experiment since the stack was exposed to the high (100 ppm) concentration of SDBS

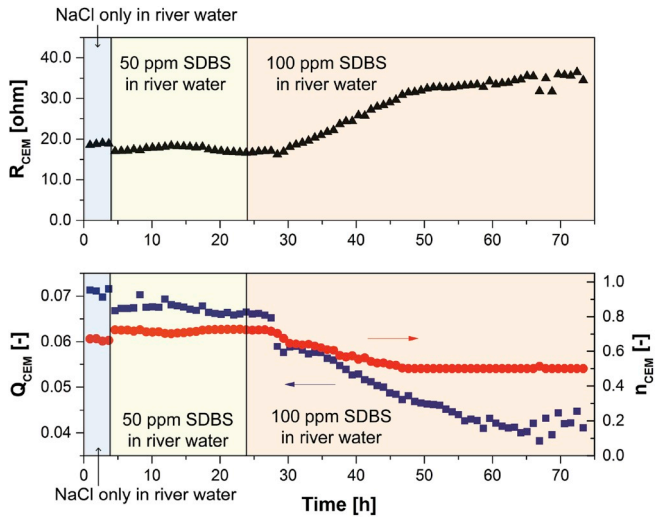

Fig. 7. (Top) Evolution of the non-ohmic CEMs resistance (values from EEC fitting of experimental data) over time during the fouling experiment. (bottom) Evolution of the non-ideal capacitance and exponent over time during the fouling experiment for the CPE associated to the CEMs. Blue background: clean river water (0.017 M NaCl). Yellow background: 0.017 M NaCl + 50 ppm SDBS in river water. Orange background: 0.017 M NaCl + 100 ppm SDBS in river water. (For interpretation of the references to colour in this figure legend, the reader is referred to the Web version of this article.)

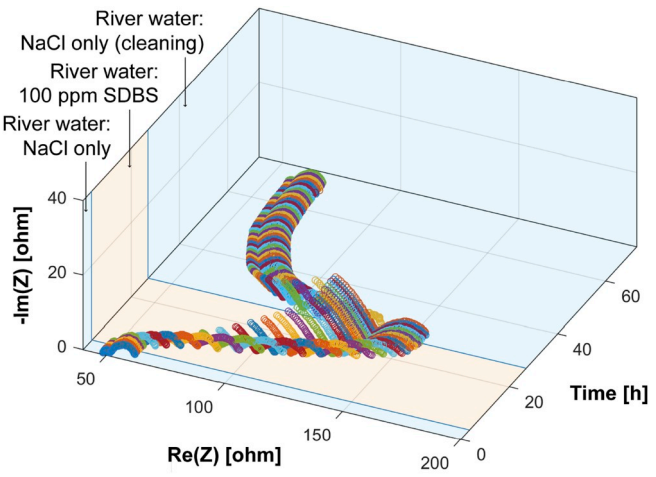

Fig. 8. Evolution of the experimental impedance data over time (Nyquist plot) during the fouling and cleaning experiment. Blue background: clean river water (0.017 M NaCl). Orange background: 0.017 M NaCl + 100 ppm SDBS in river water. (For interpretation of the references to colour in this figure legend, the reader is referred to the Web version of this article.)

from the beginning of the fouling run. Upon cleaning by flushing the stack with clean river water the electrical resistance of the stack dropped quickly and then slowly decreased until it plateaus at a higher level than the original value. Therefore, the fouling is partly irreversible. Similar results were found by Zhao et al., who reported an irreversible resistance increase after membrane fouling by sodium dodecylsulfonate (SDS) [20]. Nevertheless, DC characterizations do not give any information about the cleaning effects of the different components present in the stack, e.g. whether both membranes were cleaned or only one of them and to what extent.

Fig. 8 (Nyquist plot) and Figure S12 (Bode plots) show the evolution of the EIS spectra over time of the fouling and subsequent cleaning process.

Similar to the previous fouling experiment, upon fouling the ohmic component, and predominantly its AEM part, increased. The CEM arc was also influenced, although to a lesser extent, while fouling does not affect the arc in the centre. When the cleaning run starts, all ohmic and non-ohmic resistances decrease, but on different time scales (Figure S13). The CEM non-ohmic resistance drops significantly in the first EIS scan after the change to clean river water (Figure S14). This indicates that fouling on the CEM surface was reversible and could be easily removed, due to the electrostatic repulsion of the negative charges of SDBS and the CEM. Moreover, during cleaning, the SDBS concentration at the membrane-solution interface decreases below the CMC. The cleaning of the AEM was much slower: only after 16 h of cleaning, the arc representing the AEM in the EIS spectrum was completely recovered. This slow recovery is caused by the favorable electrostatic interaction between the negatively charged SDBS and the positively charged AEM.

Consistent with the DC results, also the EIS measurements show that there is an 11.5 Ω mismatch between the initial electrical resistance of the pristine RED stack and the stack resistance after the fouling-cleaning cycle. Opposite to the DC measurements however, the EIS spectra clearly shows that this mismatch is entirely due to an irreversible increase in the ohmic resistance so that the total stack ohmic resistance has not been fully recovered to its original value. Given that the resistance of the water compartments is the same before and after the fouling run and that the CEM was easily cleaned, this irreversible increase in ohmic resistance of the stack must be attributed to the non-reversible increase in the ohmic resistance of the AEM. This indicates that SDBS is trapped in the AEM, where it bound to the positive groups. Thus, the membrane IEC and free volume available for ion transport are not completely recovered. Further evidence of this behavior is the loss in open circuit voltage of the stack which decreased from 147 mV for the pristine stack to 143 mV after the fouling-cleaning cycle, indicating a permanent loss in permselectivity.

5. Conclusions

The reduction of the active membrane area in a RED-stack is the key to unravel fast and reliable EIS measurements at the real stack level. An EIS fouling experiment with SDBS added to river water revealed how the foulant impacted the elements of the stack on different time scales. Absorption of SDBS in the AEM leads to a fast increase in the ohmic component. SDBS domains on the AEM nucleate at low concentration and grow, thus increasing the non-ohmic component of the AEM resistance. Longer exposure times to SDBS also affect the CEM despite the unfavorable electrostatic interaction with SDBS due to the direction of the electric field towards anode and CEM. Cleaning of the stack elements at different time scales and to different extents showed that the ohmic resistance decreased slowly and plateaued at a higher level than the original. This shows that SDBS is irreversibly absorbed in the AEM, where it ion exchanges with the quaternary ammonium groups, leading to lower ion exchange capacity and free volume available for ion transport. The non-ohmic component of the AEM recovered completely, as was the case for the CEM non-ohmic resistance. However, the CEM recovered faster, thanks to the electrostatic repulsion between sulfonic acid groups and the negatively charged SDBS. The new fouling monitoring strategy presented in this work is a big step towards effective RED exploitation using natural foulants containing salinity gradients. Fouling monitoring by EIS enables the use of efficient cleaning strategies, by making use of the knowledge of which individual stack elements are susceptible to fouling and provides guidance on how to control this fouling.

Declaration of competing interest

The authors declare that they have no known competing financial interests or personal relationships that could have appeared to influence the work reported in this paper.

Acknowledgment

This work was performed in the cooperation framework of Wetsus, European Centre of Excellence for Sustainable Water Technology (www.wetsus.eu). Wetsus is co-funded by the Dutch Ministry of Economic Affairs and Ministry of Infrastructure and Environment, the Province of Fryslân, and the Northern Netherlands Provinces. This project has also received funding from the European Union's Horizon 2020 research and innovation program under the Marie Skłodowska-Curie grant agreement No 665874. The authors would like to thank the participants of the research theme "Blue Energy" for their input, suggestions and their financial support. Finally, the authors would like to express their gratitude to the Wetsus technical support team.

Appendix A. Supplementary data

Supplementary data to this article can be found online at https://doi.org/10.1016/j.jpowsour.2019.227302.

References

[1] J.W. Post, J. Veerman, H.V.M. Hamelers, G.J.W. Euverink, S.J. Metz, K. Nymeijer, C.J.N. Buisman, Salinity-gradient power: evaluation of pressure-retarded osmosis and reverse electrodialysis, J. Membr. Sci. 288 (2007) 218–230, https://doi.org/10.1016/j.memsci.2006.11.018.

[2] J.W. Post, H.V.M. Hamelers, C.J.N. Buisman, Energy recovery from controlled mixing salt and fresh water with a reverse electrodialysis system, Environ. Sci. Technol. 42 (2008) 5785–5790, https://doi.org/10.1021/es8004317.

[3] A.H. Galama, J.W. Post, H.V.M. Hamelers, V.V. Nikonenko, P.M. Biesheuvel, On the origin of the membrane potential arising across densely charged ion exchange membranes: how well does the teorell-meyer-sievers theory work? J. Membr. Sci. Res. 2 (2016) 128–140.

[4] J. Veerman, M. Saakes, S.J. Metz, G.J. Harmsen, Reverse electrodialysis: evaluation of suitable electrode systems, J. Appl. Electrochem. 40 (2010) 1461–1474, https://doi.org/10.1007/s10800-010-0124-8.

[5] E. Güler, K. Nijmeijer, Reverse electrodialysis for salinity gradient power generation: challenges and future perspectives, J. Membr. Sci. Res. 4 (2018) 108–110, https://doi.org/10.22079/JMSR.2018.86747.1193.

[6] D.A. Vermaas, D. Kunteng, M. Saakes, K. Nijmeijer, Fouling in reverse electrodialysis under natural conditions, Water Res. 47 (2013) 1289–1298, https://doi.org/10.1016/j.watres.2012.11.053.

[7] D.A. Vermaas, D. Kunteng, J. Veerman, M. Saakes, K. Nijmeijer, Periodic feedwater reversal and air sparging as antifouling strategies in reverse electrodialysis, Environ. Sci. Technol. 48 (2014) 3065–3073, https://doi.org/10.1021/es4045456.

[8] M. Vaselbehagh, H. Karkhanechi, R. Takagi, H. Matsuyama, Biofouling phenomena on anion exchange membranes under the reverse electrodialysis process, J. Membr. Sci. 530 (2017) 232–239, https://doi.org/10.1016/j.memsci.2017.02.036.

[9] D.M. Warsinger, S. Chakraborty, E.W. Tow, M.H. Plumlee, C. Bellona, S. Loutatidou, L. Karimi, A.M. Mikelonis, A. Achilli, A. Ghassemi, L.P. Padhye, S. A. Snyder, S. Curcio, C.D. Vecitis, H.A. Arafat, J.H. Lienhard, A review of polymeric membranes and processes for potable water reuse, Prog. Polym. Sci. 81 (2018) 209–237, https://doi.org/10.1016/j.progpolymsci.2018.01.004.

[10] J. Moreno, N. de Hart, M. Saakes, K. Nijmeijer, CO2saturated water as two-phase flow for fouling control in reverse electrodialysis, Water Res. 125 (2017) 23–31, https://doi.org/10.1016/j.watres.2017.08.015.

[11] E.J. Bodner, M. Saakes, T. Sleutels, C.J.N. Buisman, H.V.M. Hamelers, The RED Fouling Monitor: a novel tool for fouling analysis, J. Membr. Sci. 570–571 (2019) 294–302, https://doi.org/10.1016/j.memsci.2018.10.059.

[12] G. Di Profio, 2.13 Membranes and interfaces characterization by impedance spectroscopy, Compr. Membr. Sci. Eng. (2017) 393–410, https://doi.org/10.1016/B978-0-12-409547-2.12238-3.

[13] J.-S. Park, J.-H. Choi, J.-J. Woo, S.-H. Moon, An electrical impedance spectroscopic (EIS) study on transport characteristics of ion-exchange membrane systems, J. Colloid Interface Sci. 300 (2006) 655–662, https://doi.org/10.1016/j.jcis.2006.04.040.

[14] P. Długołecki, P. Ogonowski, S.J. Metz, M. Saakes, K. Nijmeijer, M. Wessling, On the resistances of membrane, diffusion boundary layer and double layer in ion exchange membrane transport, J. Membr. Sci. 349 (2010) 369–379, https://doi.org/10.1016/j.memsci.2009.11.069.

[15] W. Zhang, J. Ma, P. Wang, Z. Wang, F. Shi, H. Liu, Investigations on the interfacial capacitance and the diffusion boundary layer thickness of ion exchange membrane using electrochemical impedance spectroscopy, J. Membr. Sci. 502 (2016) 37–47, https://doi.org/10.1016/j.memsci.2015.12.007.

[16] A.H. Avci, P. Sarkar, R.A. Tufa, D. Messana, P. Argurio, E. Fontananova, G. Di Profio, E. Curcio, Effect of Mg^{2+}ions on energy generation by Reverse Electrodialysis, J. Membr. Sci. 520 (2016) 499–506, https://doi.org/10.1016/j.memsci.2016.08.007.

[17] E. Fontananova, D. Messana, R.A. Tufa, I. Nicotera, V. Kosma, E. Curcio, W. van Baak, E. Drioli, G. Di Profio, Effect of solution concentration and composition on the electrochemical properties of ion exchange membranes for energy conversion, J. Power Sources 340 (2017) 282–293, https://doi.org/10.1016/j.jpowsour.2016.11.075.

[18] J.-S. Park, J.-H. Choi, K.-H. Yeon, S.-H. Moon, An approach to fouling characterization of an ion-exchange membrane using current-voltage relation and electrical impedance spectroscopy, J. Colloid Interface Sci. 294 (2006) 129–138, https://doi.org/10.1016/j.jcis.2005.07.016.

[19] H.J. Lee, M.K. Hong, S.D. Han, J. Shim, S.H. Moon, Analysis of fouling potential in the electrodialysis process in the presence of an anionic surfactant foulant, J. Membr. Sci. 325 (2008) 719–726, https://doi.org/10.1016/j.memsci.2008.08.045.

[20] Z. Zhao, S. Shi, H. Cao, Y. Li, Electrochemical impedance spectroscopy and surface properties characterization of anion exchange membrane fouled by sodium dodecyl sulfate, J. Membr. Sci. 530 (2017) 220–231, https://doi.org/10.1016/j.memsci.2017.02.037.

[21] Z. Zhao, S. Shi, H. Cao, B. Shan, Y. Sheng, Property characterization and mechanism analysis on organic fouling of structurally different anion exchange membranes in electrodialysis, Desalination 428 (2018) 199–206, https://doi.org/10.1016/j.desal.2017.11.021.

[22] I. Choi, J.Y. Han, S.J. Yoo, D. Henkensmeier, J.Y. Kim, S.Y. Lee, J. Han, S.W. Nam, H.-J. Kim, J.H. Jang, Experimental investigation of operating parameters in power generation by lab-scale reverse electro-dialysis (RED), Bull. Korean Chem. Soc. 37 (2016) 1010–1019, https://doi.org/10.1002/bkcs.10810.

[23] V.V. Nikonenko, A.E. Kozmai, Electrical equivalent circuit of an ion-exchange membrane system, Electrochim. Acta 56 (2011) 1262–1269, https://doi.org/10.1016/j.electacta.2010.10.094.

[24] P. Sistat, A. Kozmai, N. Pismenskaya, C. Larchet, G. Pourcelly, V. Nikonenko, Low-frequency impedance of an ion-exchange membrane system, Electrochim. Acta 53 (2008) 6380–6390, https://doi.org/10.1016/j.electacta.2008.04.041.

[25] H.-J. Lee, M.-K. Hong, S.-D. Han, J. Shim, S.-H. Moon, Analysis of fouling potential in the electrodialysis process in the presence of an anionic surfactant foulant, J. Membr. Sci. 325 (2008) 719–726, https://doi.org/10.1016/j.memsci.2008.08.045.

[26] H.-J. Lee, M.-K. Hong, S.-D. Han, S.-H. Cho, S.-H. Moon, Fouling of an anion exchange membrane in the electrodialysis desalination process in the presence of organic foulants, Desalination 238 (2009) 60–69, https://doi.org/10.1016/j.desal.2008.01.036.

[27] J. Veerman, M. Saakes, S.J. Metz, G.J. Harmsen, Reverse electrodialysis: performance of a stack with 50 cells on the mixing of sea and river water, J. Membr. Sci. 327 (2009) 136–144, https://doi.org/10.1016/j.memsci.2008.11.015.

[28] D.A. Vermaas, J. Veerman, M. Saakes, K. Nijmeijer, Influence of multivalent ions on renewable energy generation in reverse electrodialysis, Energy Environ. Sci. 7 (2014) 1434–1445, https://doi.org/10.1039/c3ee43501f.

[29] J. Moreno, V. Díez, M. Saakes, K. Nijmeijer, Mitigation of the effects of multivalent ion transport in reverse electrodialysis, J. Membr. Sci. 550 (2018) 155–162, https://doi.org/10.1016/j.memsci.2017.12.069.

[30] J.-L. Dellis, Zfit, MATLAB cent. File exch. https://nl.mathworks.com/matlabcentral/fileexchange/19460-zfit, 2010. (Accessed 11 September 2018).

[31] Z. Zhao, S. Shi, H. Cao, B. Shan, Y. Sheng, Property characterization and mechanism analysis on organic fouling of structurally different anion exchange membranes in electrodialysis, Desalination 428 (2018) 199–206, https://doi.org/10.1016/j.desal.2017.11.021.